Electronic Supplementary Material (ESI) for Environmental Science: Nano.

Supporting Information

Towards broad-operation window for stable CO_2 electroreduction to HCOOH by upcycling design of electroplating sludge derived Sn@N/P-doped carbon

Xiaohui Zhong[a], Zuqi Zhong[a], Shujie Liang[a], Gongchang Zeng[a], Shuang Cheng[a], Hong Deng*[a,b], Zhang Lin[a,c]

[a] School of Environment and Energy, Guangdong Provincial Key Laboratory of Solid Wastes Pollution Control and Recycling, The Key Laboratory of Pollution Control and Ecosystem Restoration in Industry Clusters (Ministry of Education), South China University of Technology, Guangzhou, Guangdong 510006, China

[b] Guangdong Engineering and Technology Research Center for Environmental Nanomaterials, South China University of Technology, Guangzhou, Guangdong 510006, China

[c] Chinese National Engineering Research Center for Control & Treatment of Heavy Metal Pollution, School of Metallurgy and Environment, Central South University, Changsha 410083, China

* Correspondence Author: Hong Deng; E-mail: dengh2016@scut.edu.cn

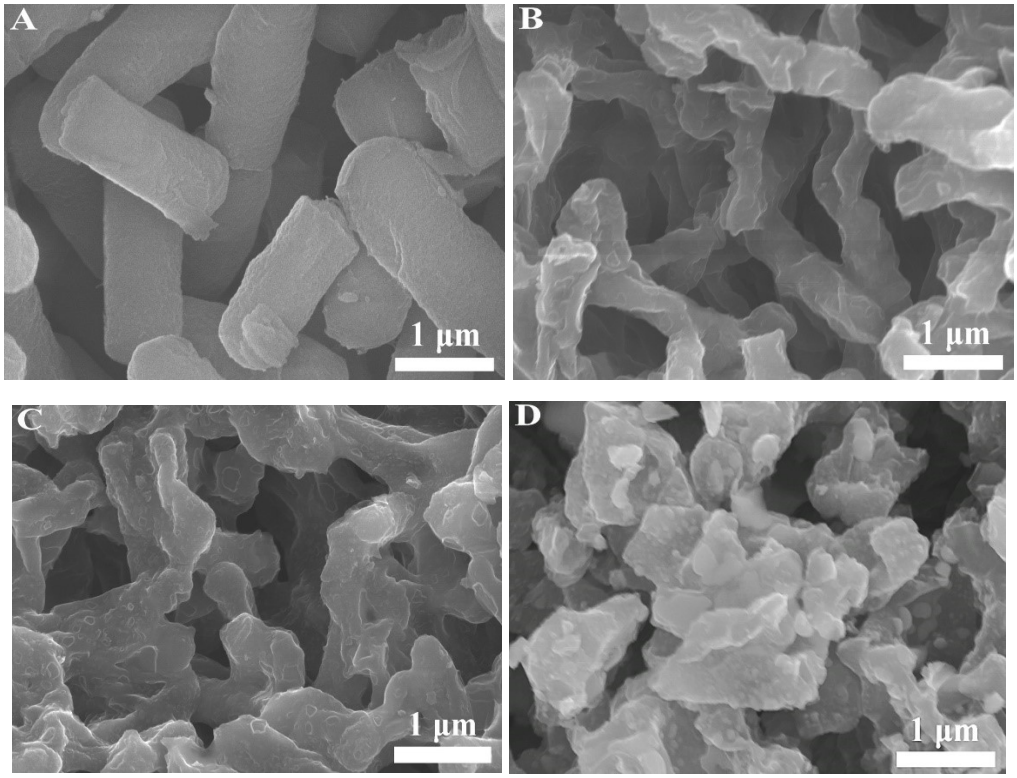

Fig. S1 FE-SEM images of (A) Sn@BS and Sn@NPC at (B) 500℃, (C) 600℃, (D) 800℃.

Fig. S1 showed the microscopic morphology of the Sn@BS precursor at different calcination temperatures. The morphology of the bacterial carrier was well maintained in the range of 700°C (**Fig. 1D**). When the temperature reached 800°C, the morphology was completely broken.

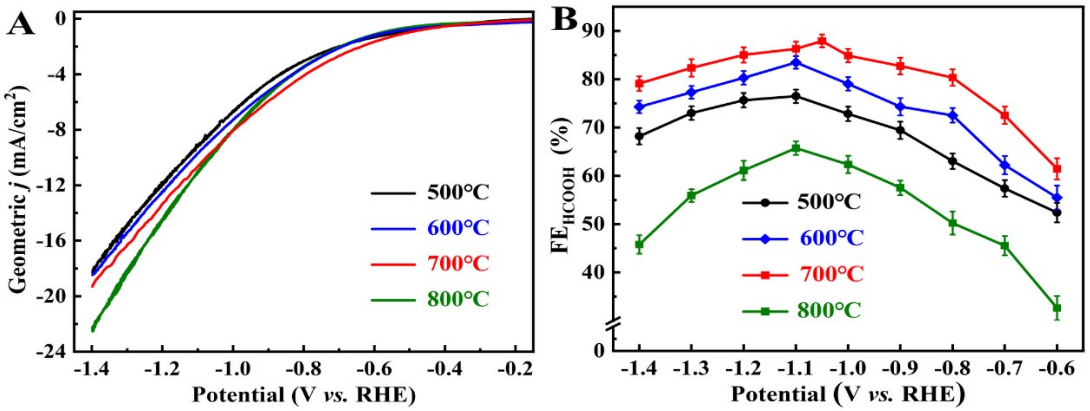

Fig. S2 (A) LSV curves and (B) Faradaic efficiencies of Sn@NPC at different calcination temperatures.

To make sure the best performance at different temperatures, the current density and Faraday efficiency of formate were tested. The Faradaic efficiency of formate increased with the increase of temperature. However, when the temperature reached 800°C, the Faradaic efficiency decreased significantly, which could be due to its morphological fragmentation.

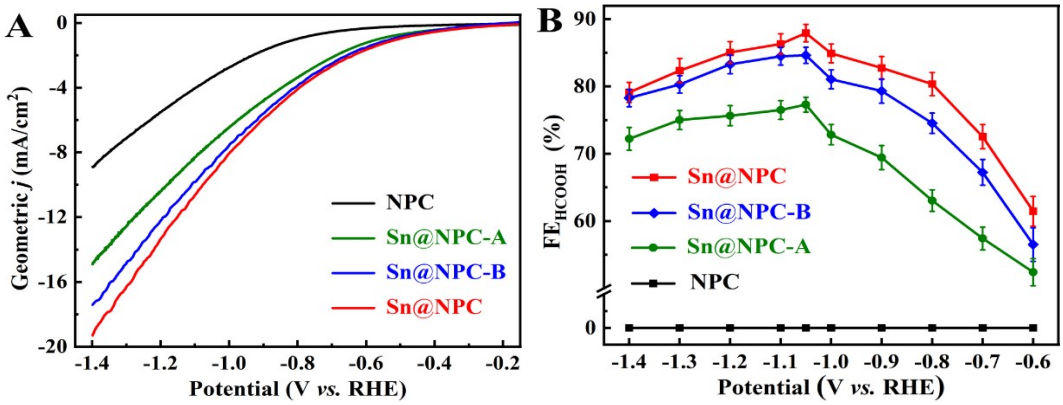

Fig. S3 (A) LSV curves and (B) Faradaic efficiencies of HCOOH for Sn@NPC-A, Sn@NPC-B, Sn@NPC and NPC measured in CO_2 saturated 0.1 M $KHCO_3$ solution.

The performance of CO_2RR might be affected by the tin loading. From **Fig. S3**, the performance of CO_2RR-to-HCOOH gradually increased with the increasing of tin content. However, an optimal CO_2RR performance was obtained for Sn@NPC due to the adsorption saturation of bacteria. Therefore, all subsequent tests were mainly carried out on Sn@NPC composites.

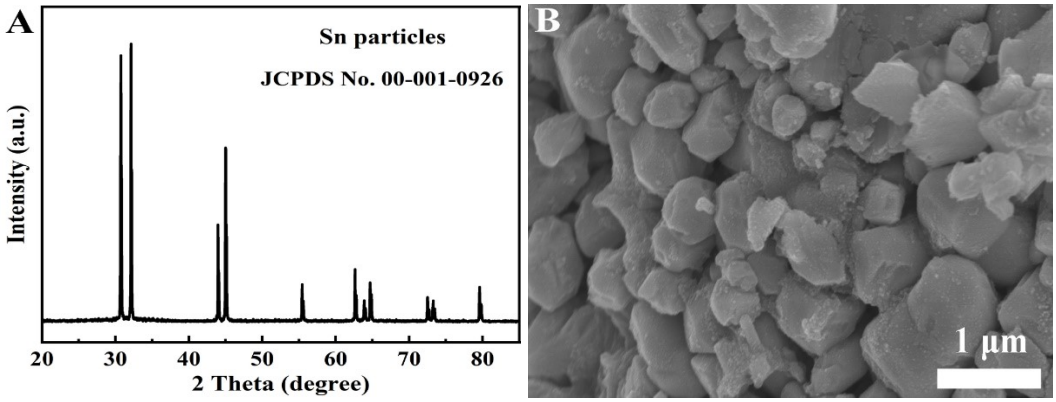

Fig. S4 (A) XRD pattern and (B) FESEM image of Sn particles.

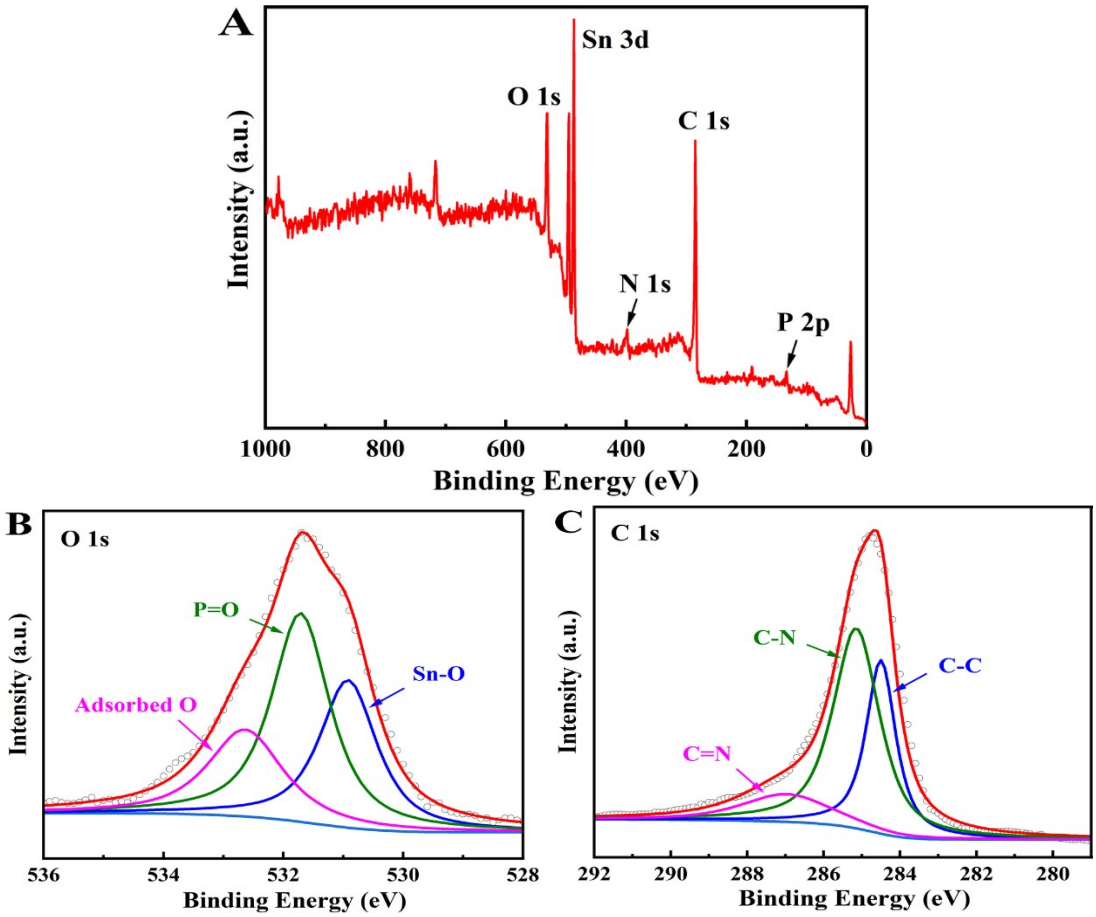

Fig. S5 (A) XPS survey spectrum of Sn@NPC. High resolution XPS spectrum of (B) O 1s and (C) C 1s collected from Sn@NPC composites.

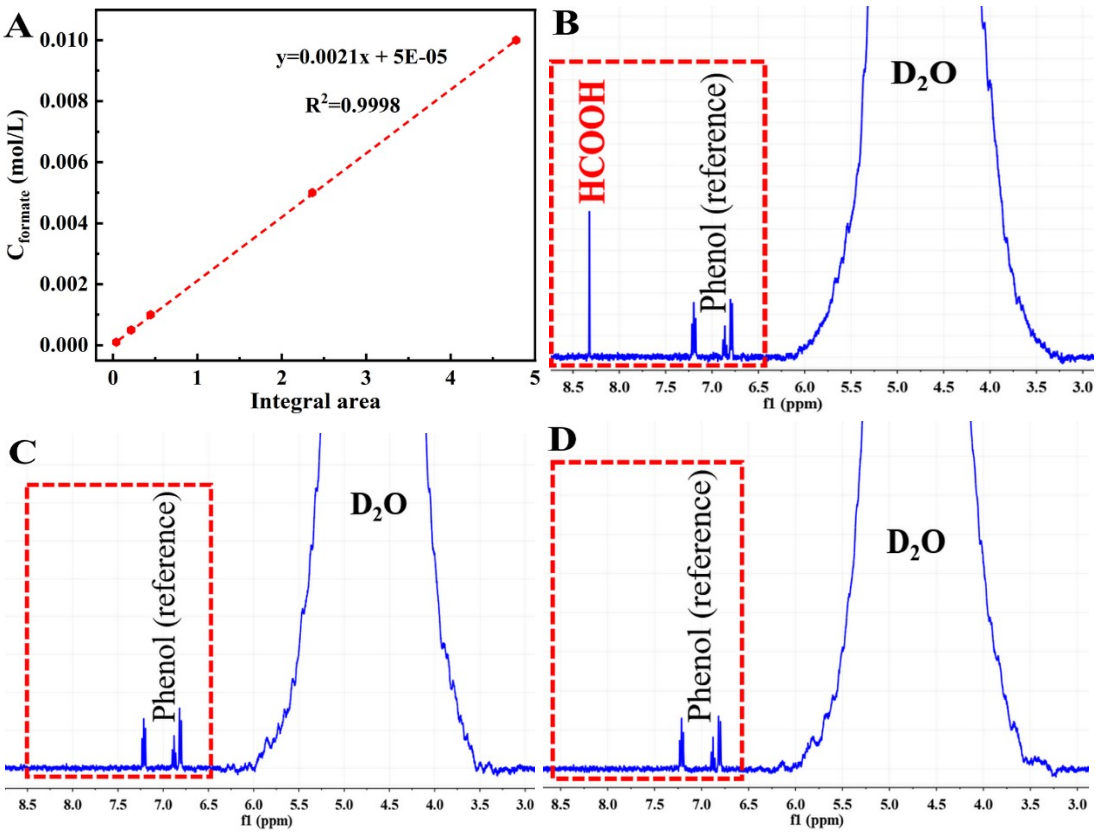

Fig. S6 (A) Calibration curve for quantifying HCOOH concentration by Nuclear magnetic resonance (^{1}H-NMR) with phenol as the internal standard; NMR results after CO_2RR for Sn@NPC in (B) CO_2-saturated condition and (C) Ar-saturated condition; (D) NMR result after CO_2RR for NPC in CO_2-saturated condition.

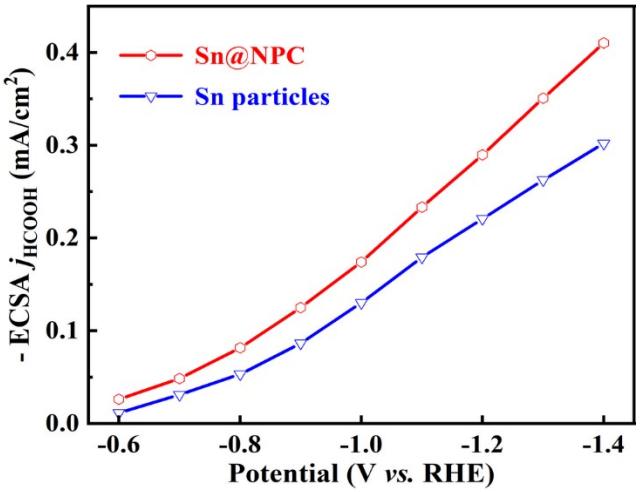

Fig. S7 ECSA-normalized partial current densities of HCOOH *vs.* applied potentials.

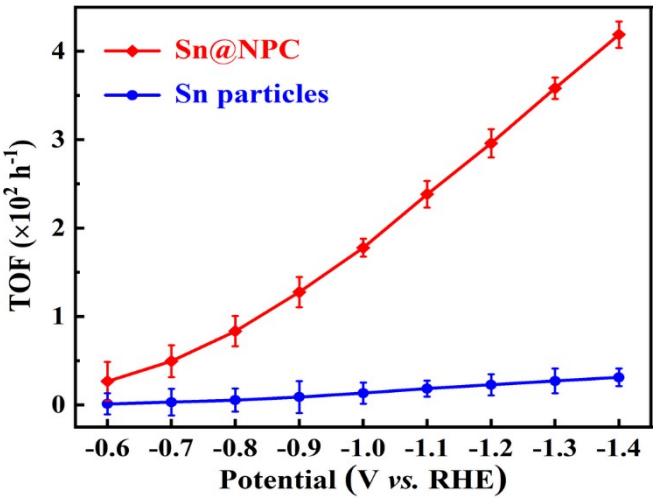

Fig. S8 TOF curves of Sn@NPC and Sn particles at different applied potential.

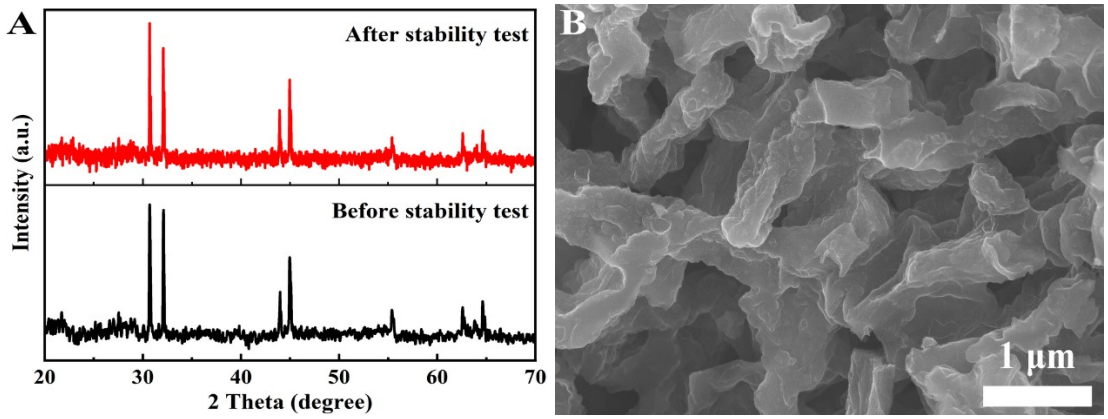

Fig. S9 (A) XRD patterns for Sn@NPC before and after 105 h stability measurement; (B) FESEM image of Sn@NPC after stability measurement.

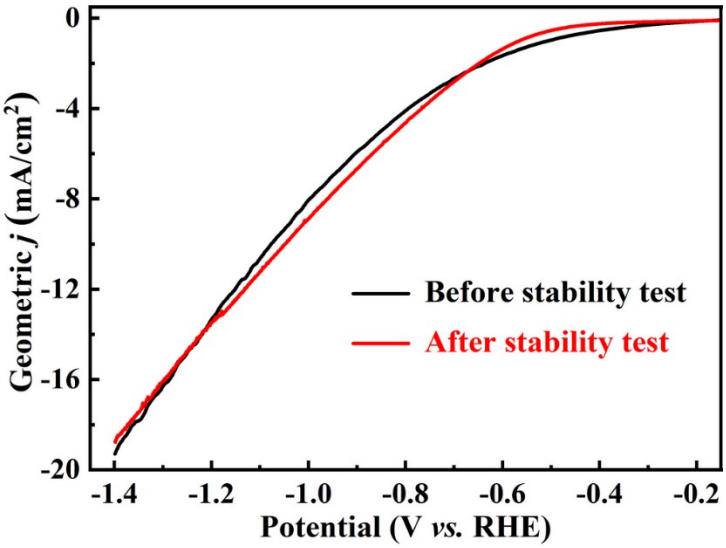

Fig. S10 LSV curves for Sn@NPC before and after stability test under CO_2-saturated 0.1 M $KHCO_3$ aqueous solution.

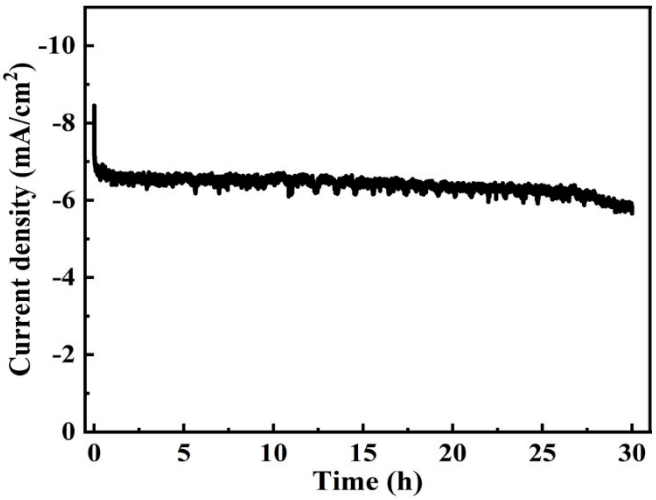

Fig. S11 Stability measurement of Sn particles at -1.0 V *vs.* RHE in CO_2-saturated 0.1 M $KHCO_3$ aqueous solution.

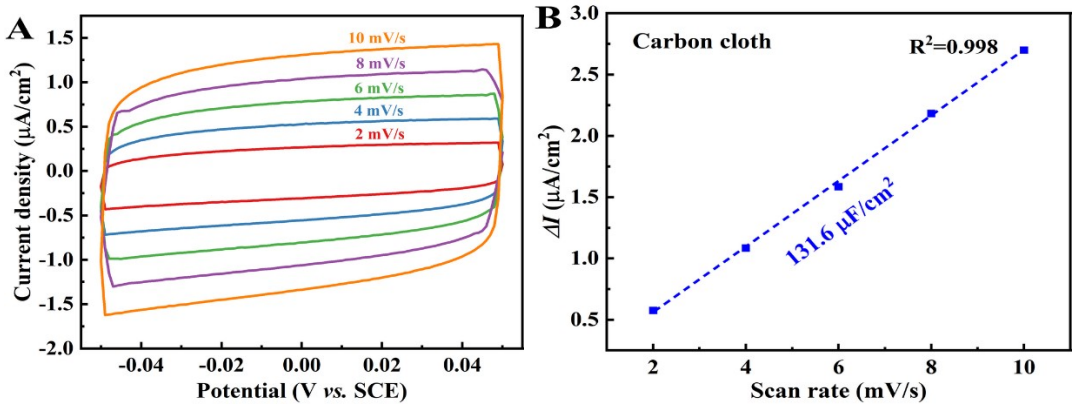

Fig. S12 (A) CV curves measured in a non-Faradaic region at various scan rates for carbon cloth; (B) Charging current density differences plotted against scan rates.

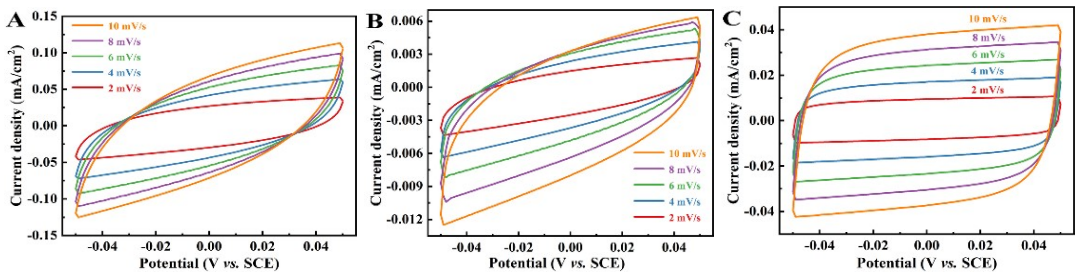

Fig. S13 CV curves measured in a non-Faradaic region at various scan rates for (A) Sn@NPC, (B) NPC and (C) Sn particles.

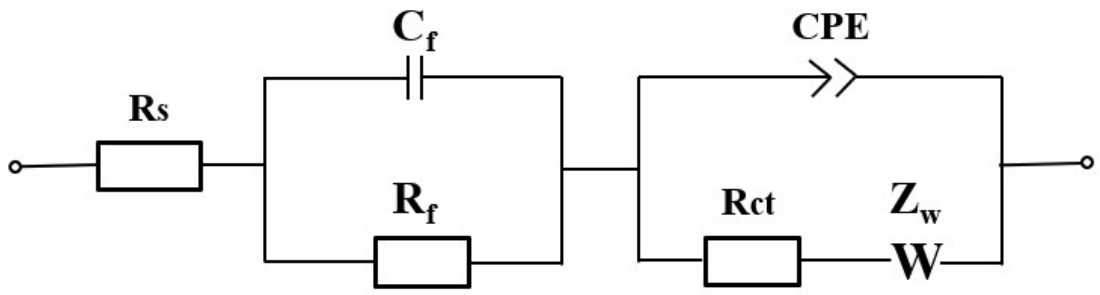

Fig. S14 The proposed equivalent circuit based on EIS tests.

Table S1 The fitted results of EIS data using the equivalent circuit in **Fig. 4B**.

Electrode	R_s (Ω)	R_{ct} (Ω)	R_f (Ω)
NPC	6.85	101.56	84.57
Sn particles	6.53	47.48	58.18
Sn@NPC	6.59	36.04	51.44

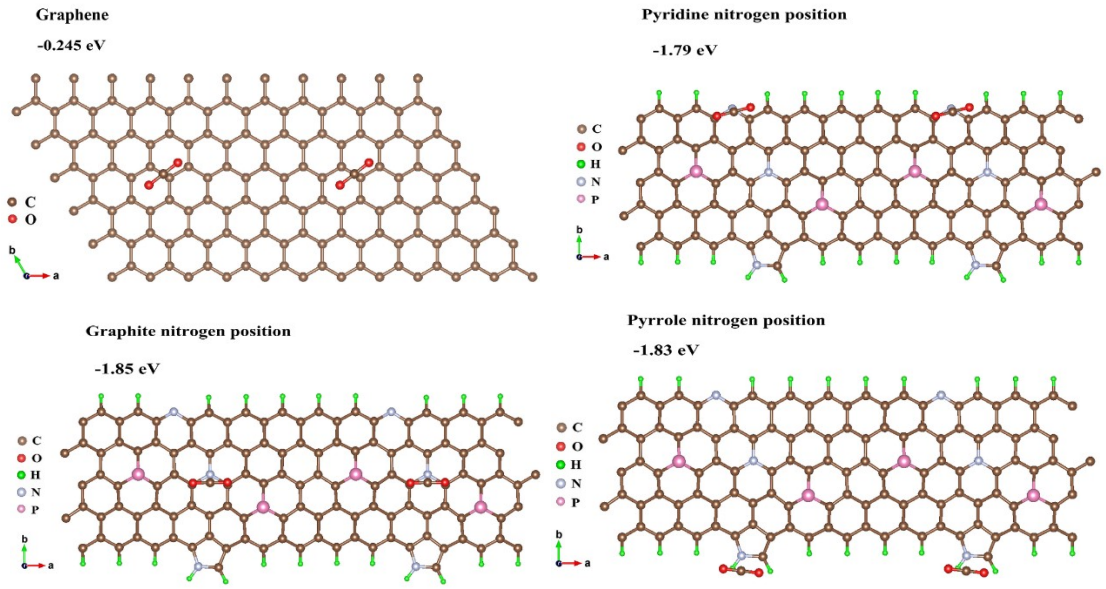

Fig. S15 DFT calculated CO_2 adsorption models of graphene, N/P-doped graphene and their corresponding adsorption energies.

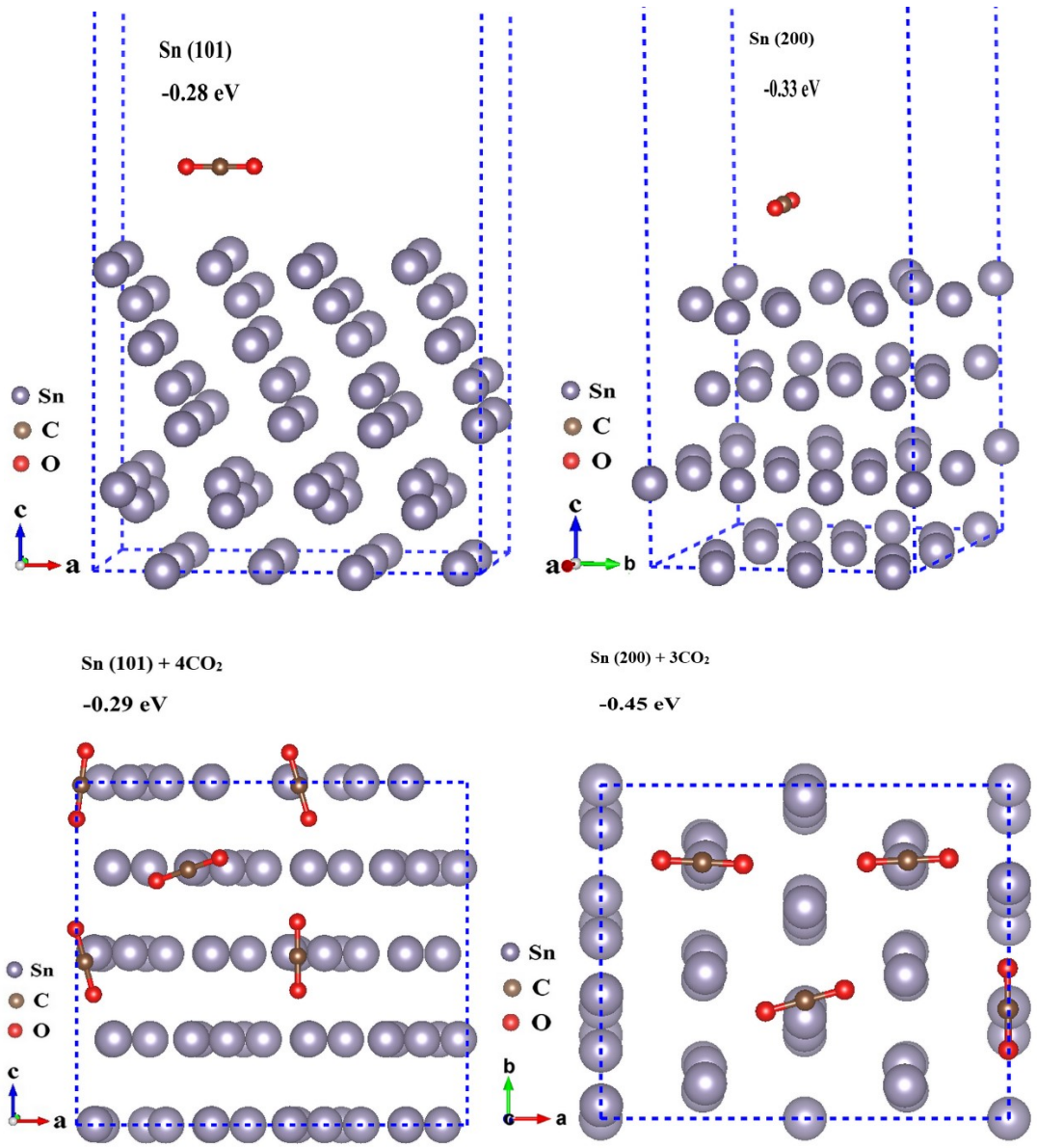

Fig. S16 DFT calculated CO_2 adsorption models of Sn(101), Sn(200) with/without their surfaces initially covered by four or three physiosorbed CO_2 molecules.

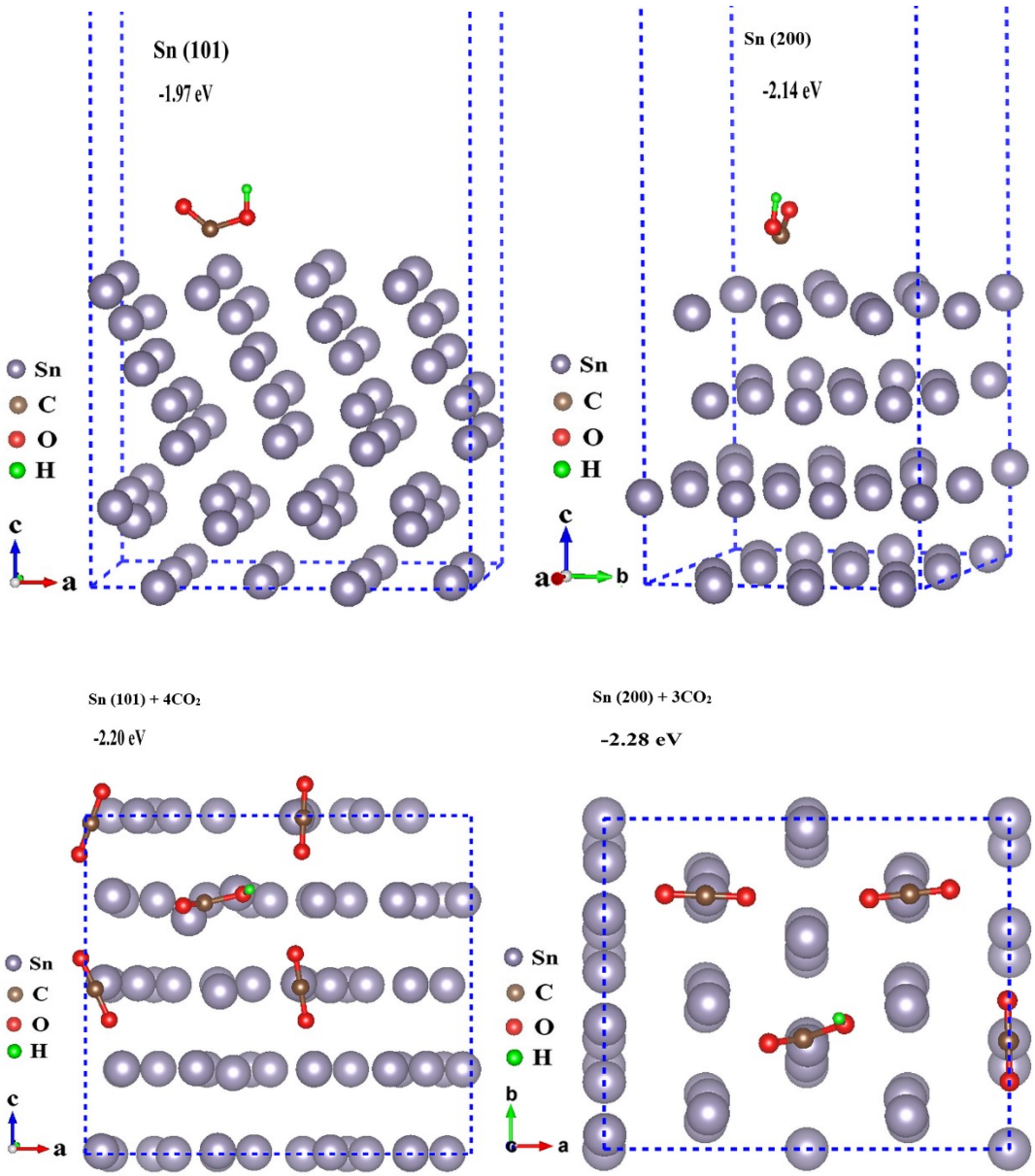

Fig. S17 DFT calculated *COOH adsorption models of Sn(101), Sn(200) with/without their surfaces initially covered by four or three physiosorbed CO_2 molecules.

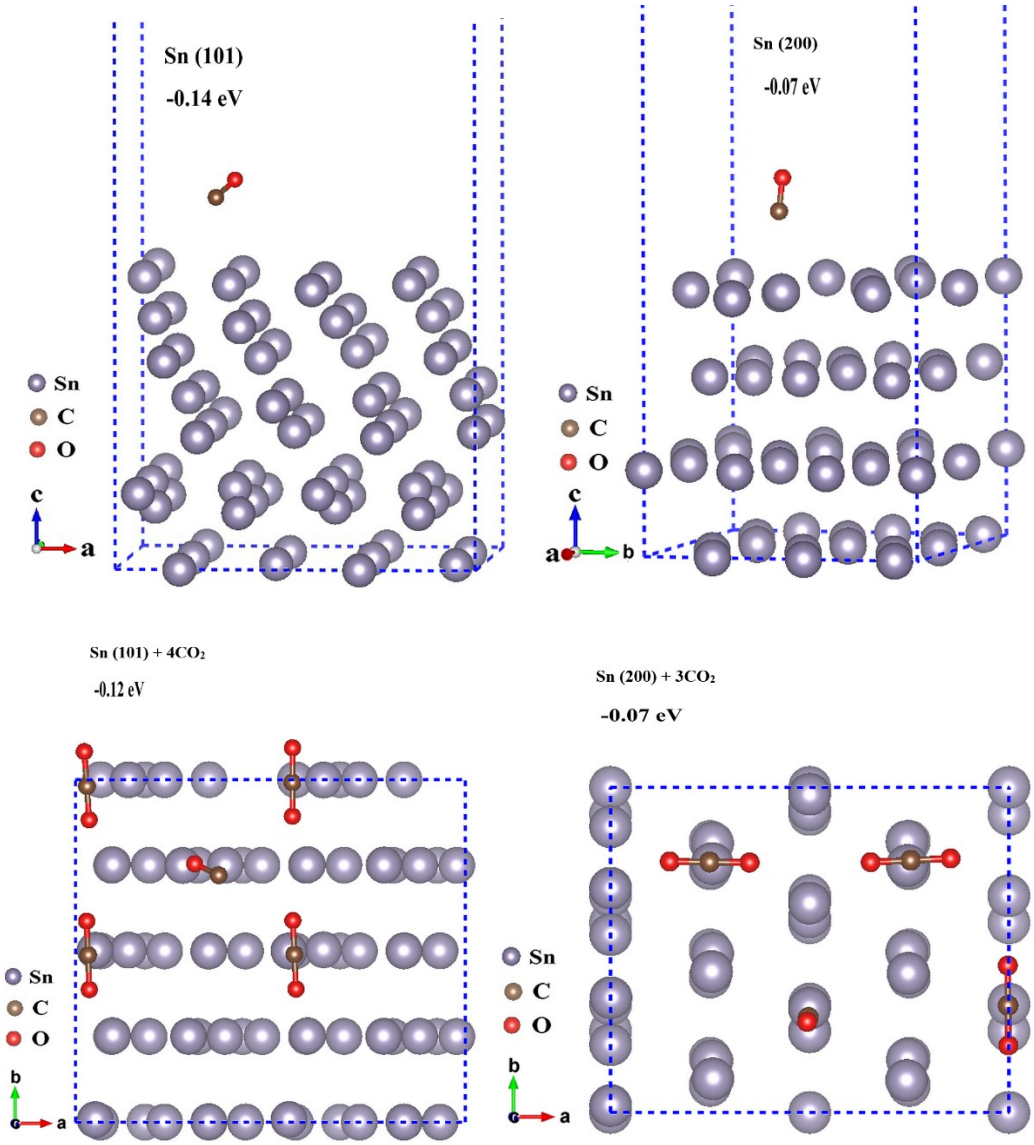

Fig. S18 DFT calculated *CO adsorption models of Sn(101), Sn(200) with/without their surfaces initially covered by four or three physiosorbed CO_2 molecules.

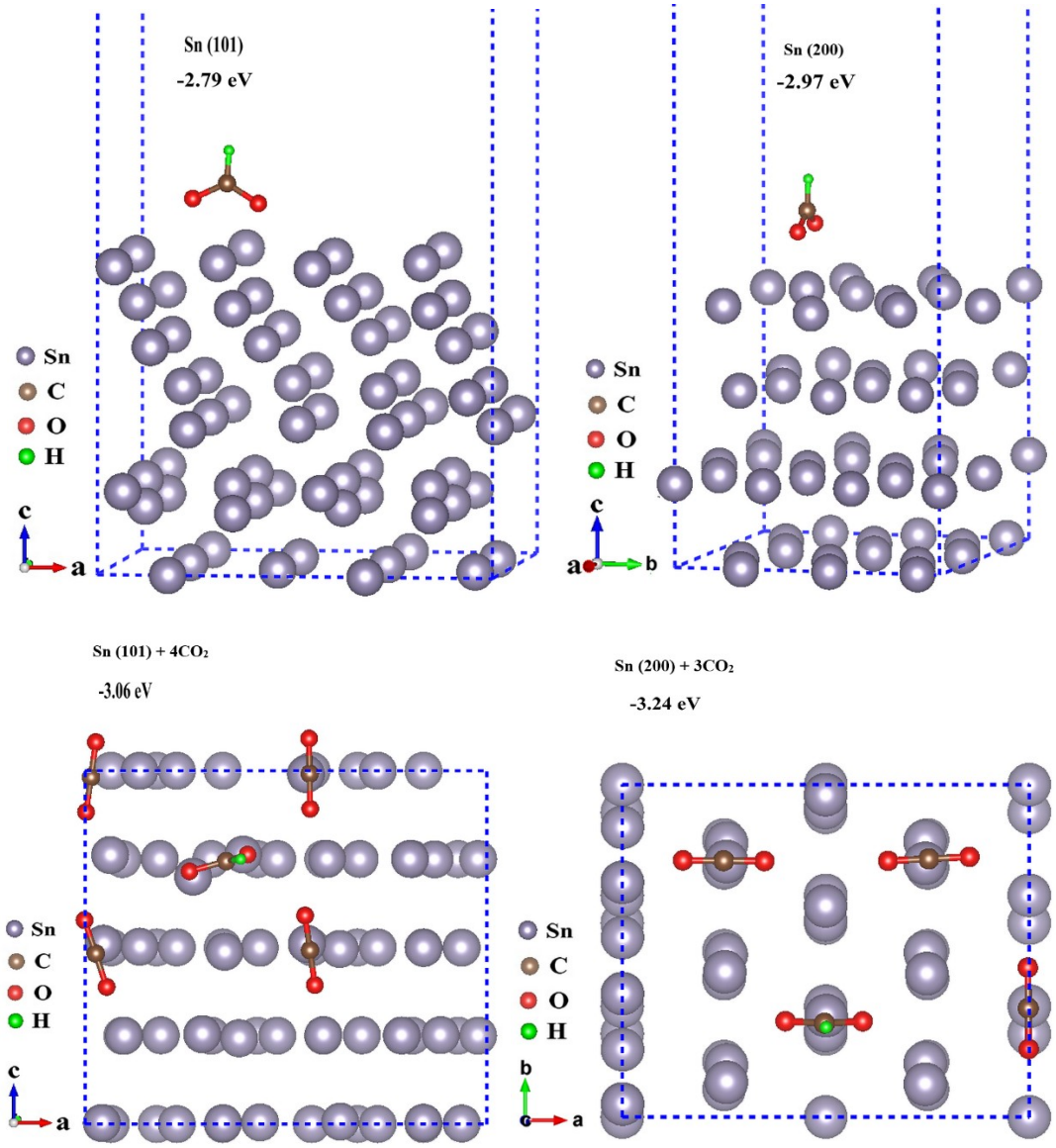

Fig. S19 DFT calculated *OCHO adsorption models of Sn(101), Sn(200) with/without their surfaces initially covered by four or three physiosorbed CO_2 molecules.

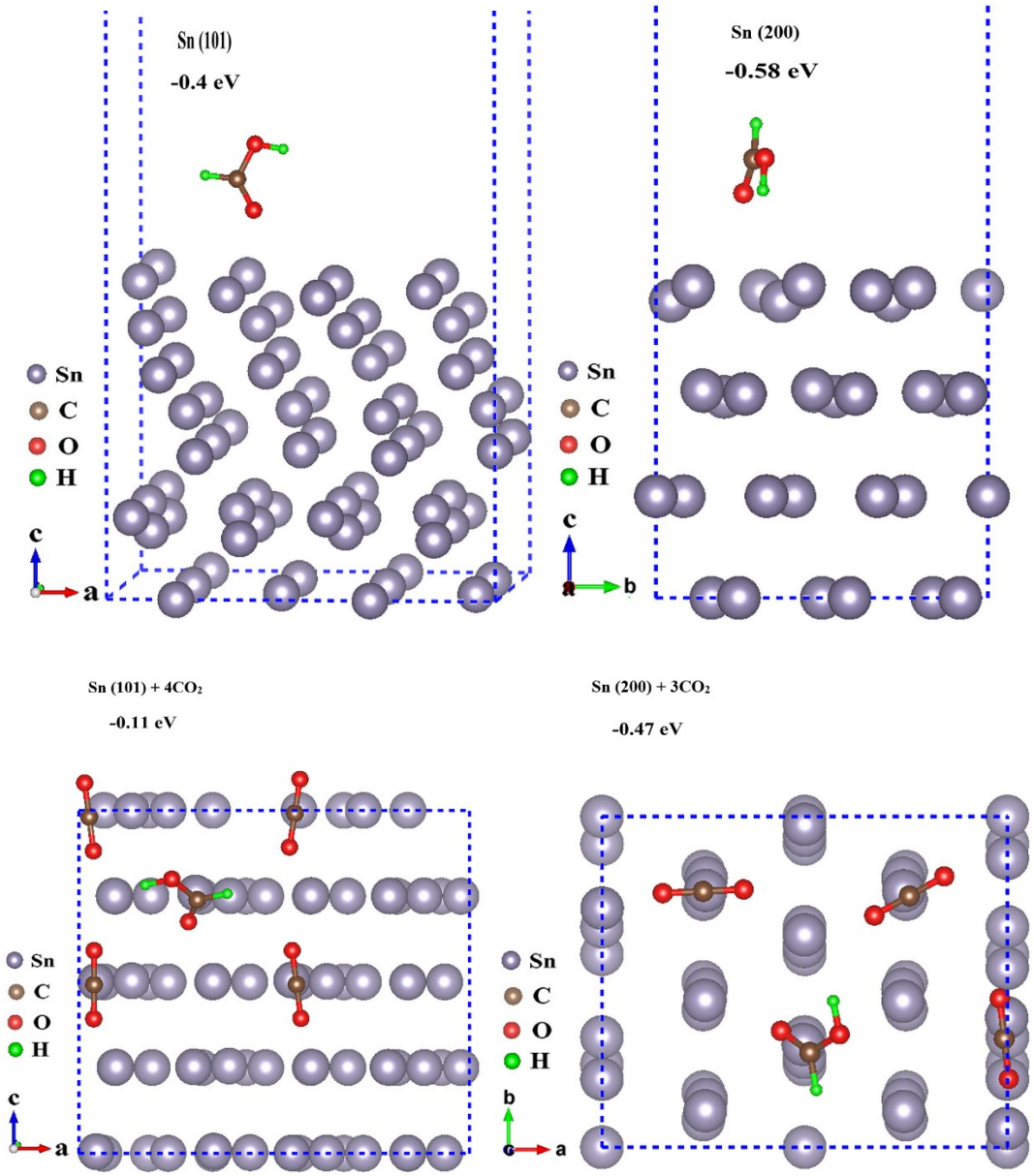

Fig. S20 DFT calculated *HCOOH adsorption models of Sn(101), Sn(200) with/without their surfaces initially covered by four or three physiosorbed CO_2 molecules.

Table S2 The ICP- OES results of electroplating sludge extracting solution.

Element	Sn	Fe	Si	Na
Weight %	58.75	19.14	12.97	9.08

Table S3 The concentrations of tin for the different samples were analyzed *via* ICP-OES.

Name	Mass $_{sludge}$ (g)	C_{Sn} (ppm)	Sn (wt %)
Sn@NPC-A	0.3	1763	21.47
Sn@NPC-B	0.4	2350	31.11
Sn@NPC	0.5	2937	31.43

Table S4 Comparison of the electrocatalytic performance for CO_2RR to formate of recently reported Sn-based electrocatalysts.

Catalysts	Electrolyte ($KHCO_3$)	E (V *vs.* RHE)	J_{HCOOH} (mA/cm^2)	FE_{Max} (%)	Stability (h)	Ref.
Wavy SnO_2	0.5 M	-1.0	22	87.4	18	1
Porous SnO_2 nanosheets	0.5 M	-0.7	2.31*	92.4	10	2
SnO_2 porous nanowires	0.1 M	-1.0	8*	~80	15	3
Mesoporous SnO_2 nanosheets	0.5 M	-1.3	7.47*	90	12	4
Sn/SnO/SnO_2 nanosheets	0.5 M	-0.9	17.1	89.6	10	5
Porous Sn foam	0.1 M	-0.9	~7.65*	95.6	55	6
SnS_2 monolayers	0.1 M	-0.8	—	94	80	7
Sn/Reduced Graphene Oxide	0.1 M	-1.02*	~24*	98	—	8
H-SnS_2 nanosheets	0.1 M	-0.9	~18.6	87	—	9
$SnSe_2$@CC	0.1 M	-0.76	12	88.4	10	10
Sn quantum sheets	0.1 M	-1.1*	18.69*	89	50	11
Sn@NPC	**0.1 M**	**-1.05**	**8.05**	**87.93**	**105**	**This work**

*: The values were obtained from literature estimation.

References

1 Z. Chen, T. Fan, Y.-Q. Zhang, J. Xiao, M. Gao, N. Duan, J. Zhang, J. Li, Q. Liu, X. Yi, J.-L. Luo, Wavy SnO_2 catalyzed simultaneous reinforcement of carbon dioxide adsorption and activation towards electrochemical conversion of CO_2 to HCOOH, *Appl. Catal. B Environ.*, 2020, **261**, 118243.

2 G. Liu, Z. Li, J. Shi, K. Sun, Y. Ji, Z. Wang, Y. Qiu, Y. Liu, Z. Wang, P. Hu, Black reduced porous SnO_2 nanosheets for CO_2 electroreduction with high formate selectivity and low overpotential, *Appl. Catal. B Environ.*, 2020, **260**, 118134.

3 B. Kumar, V. Atla, J.P. Brian, S. Kumari, T.Q. Nguyen, M. Sunkara, J.M. Spurgeon, Reduced SnO_2 porous nanowires with a high density of grain boundaries as catalysts for efficient electrochemical CO_2-into-HCOOH conversion, *Angew. Chem. Int. Ed.*, 2017, **56**, 3645-3649.

4 F. Wei, T. Wang, X. Jiang, Y. Ai, A. Cui, J. Cui, J. Fu, J. Cheng, L. Lei, Y. Hou, S. Liu, Controllably engineering mesoporous surface and dimensionality of SnO_2 toward high-performance CO_2 electroreduction, *Adv. Funct. Mater.*, 2020, **30**, 2002092.

5 J. Wu, X. Bai, Z. Ren, S. Du, Z. Song, L. Zhao, B. Liu, G. Wang, H. Fu, Multivalent Sn species synergistically favours the CO_2-into-HCOOH conversion, *Nano Res*., 2020, **14**, 1053-1060.

6 D. Li, J. Wu, T. Liu, J. Liu, Z. Yan, L. Zhen, Y. Feng, Tuning the pore structure of porous tin foam electrodes for enhanced electrochemical reduction of carbon dioxide to formate, *Chem. Eng. J.*, 2019, **375**, 122024.

7 J. He, X. Liu, H. Liu, Z. Zhao, Y. Ding, J. Luo, Highly selective electrocatalytic reduction of CO_2 to formate over Tin(IV) sulfide monolayers, *J. Catal.*, 2018, **364**, 125-130.

8 T. Tsujiguchi, Y. Kawabe, S. Jeong, T. Ohto, S. Kukunuri, H. Kuramochi, Y. Takahashi, T. Nishiuchi, H. Masuda, M. Wakisaka, K. Hu, G. Elumalai, J.-i. Fujita, Y. Ito, Acceleration of electrochemical CO_2 reduction to formate at the Sn/reduced graphene oxide interface, *ACS Catal.*, 2021, **11**, 3310-3318.

9 A. Zhang, Y. Liang, H. Li, S. Wang, Q. Chang, K. Peng, Z. Geng, J. Zeng, Electronic tuning of SnS_2 nanosheets by hydrogen incorporation for efficient CO_2 electroreduction, *Nano Lett.*, 2021, **21**, 7789-7795.

10 B. He, L. Jia, Y. Cui, W. Zhou, J. Sun, J. Xu, Q. Wang, L. Zhao, $SnSe_2$ nanorods on carbon cloth as a highly selective, active, and flexible electrocatalyst for electrochemical reduction of CO_2 into formate, *ACS Appl. Energy Mater.*, 2019, **2**, 7655-7662.

11 F. Lei, W. Liu, Y. Sun, J. Xu, K. Liu, L. Liang, T. Yao, B. Pan, S. Wei, Y. Xie, Metallic tin quantum sheets confined in graphene toward high-efficiency carbon dioxide electroreduction, *Nat. Commun.*, 2016, **7**, 12697.